

Tropospheric Response in the Antarctic Circumpolar Wave along the Sea Ice Edge around Antarctica

Warren B. White

Scripps Institution of Oceanography, University of California, San Diego, La Jolla, California

Per Gloersen

Oceans and Ice Branch, Laboratory for Hydrosphere Sciences, NASA Goddard Space Flight Center, Greenbelt, Maryland

Ian Simmonds

School of Earth Sciences, University of Melbourne, Parkville, Victoria, Australia

(Manuscript received 27 March 2003, in final form 5 December 2003)

ABSTRACT

The Antarctic circumpolar wave (ACW) signal of a 3.7-yr period occurs along the sea ice edge forming around Antarctic each fall–winter–spring from 1982 to 2001. It was larger during the first decade than the second and has retracted sea ice extent (SIE) anomalies coinciding with warmer sea surface temperature, greater upward latent heat flux, and higher precipitation, driving deep convection in the troposphere associated with low-level convergence and upper-level divergence. Lower sea level pressure is displaced 90° of phase to the west of retracted SIE anomalies, coinciding with increased extratropical cyclone density and intensity. The authors diagnose tropospheric thermal and potential vorticity budgets of this ACW signal using NCEP–NCAR reanalysis datasets, which show retracted SIE anomalies driving upper-level diabatic heating and low-level cooling, the former (latter) balanced mainly by vertical heat advection (poleward heat advection). This explains the anomalous poleward surface winds and deep convection observed over retracted SIE anomalies in this ACW signal. Thus, the vertical gradient of diabatic heating is balanced mainly by horizontal vortex tube advection at the low level and horizontal absolute vorticity advection at the upper level, together yielding the anomalous equivalently barotropic poleward wind response to the retracted SIE anomaly. Anomalous SIE-induced deep convection at the sea ice edge drives anomalous zonal (Walker-like) cells that teleconnect opposite phases in the ACW signal. It also drives anomalous Ferrell cells that teleconnect the ACW signal along the sea ice edge to that along the Subtropical Front near 35°S.

relative vorticity (a). At this level, the net vortex tube advection terms on the left-hand side of [Eq. (7.1) (terms b, e, and f in Fig. 5)] mostly cancel one another, while the mean advection of anomalous relative vorticity of $\sim 16 \times 10^{-12} \text{ s}^{-2}$ dominates the anomalous meridional advection of planetary vorticity by $\sim -7 \times 10^{-12} \text{ s}^{-2}$. Thus, the anomalous SIE-induced upper-level circulation derives mainly from consideration of the vorticity balance.

8. Anomalous Ferrell cells and zonal (Walker-like) cells in the ACW

The anomalous SIE-induced ascending motion in the ACW along the sea ice edge in fall–winter–spring (Fig. 4f) are connected to neighboring SIE-induced descending motion via divergent wind anomalies (V_D). To demonstrate this, we display a short animation sequence of the zonal vertical section of divergent wind anomalies in the ACW along the fall–winter–spring sea ice edge (defined by the 50% SIC criterion), extending zonally around the globe from 30° to 30°E each year for 3 yr from 1986 to 1988 (Fig. 6). Also displayed are the corresponding zonal profiles of the anomalous $-SIE$ in the ACW along the sea ice edge, with retracted SIE anomalies positive. Here, we find anomalous ascending (descending) motion occurring nominally over the retracted (expanded) SIE anomalies, forming zonal circulation cells in the troposphere along the sea ice edge that are similar to zonal Walker cells in the Tropics (Bjerknes 1969). Moreover, we find the eastward propagation of SIE anomalies in the ACW over the 3 yr accompanied by eastward propagation of the corresponding zonal (Walker-like) cells, which connect corresponding anomalous ascending and descending motion along the sea ice edge. In these anomalous zonal cells, vertical wind speeds range over $\pm 0.0013 \text{ m s}^{-1}$, while zonal divergent wind speeds range over $\pm 0.40 \text{ m s}^{-1}$. Some of the anomalous zonal cells extend vertically from the low level near 900 hPa into the lower stratosphere above 200 hPa, while others extend from the low to midlevel near 500 hPa.

Next, we display the meridional vertical section of divergent wind anomalies in the ACW along 180° longitude, extending from the Ross Sea to New Zealand for 1986 and 1988 (Fig. 7). These two realizations show covarying warm (cool) SST adjacent to the sea ice edge and inferred retracted (expanded) SIE anomalies along the sea ice edge, associated with cool (warm) SST anomalies at the Subtropical Front near 30°S . In these anomalous Ferrell cells, vertical wind speeds range over $\pm 0.0013 \text{ m s}^{-1}$ while meridional divergent wind speeds range over $\pm 0.55 \text{ m s}^{-1}$. Thus, the ACW along the Subtropical Front near 30°S in the western Pacific sector is teleconnected to the ACW along the sea ice edge near 63°S in the Ross Sea via these anomalous Ferrell cells.

9. Discussion and conclusions

The ACW signal near the 3.7-yr period dominates the SAM signal near the 1.0-yr period and the three other ACW signals at the 2.9-, 7.1-, and 17-yr periods in explaining $\sim 50\%$ of the variance in winter SIC anomalies in the Ross and Weddell Seas from 1983 to 1992. Here, we examined the troposphere response to SIE anomalies in this 3.7-yr period ACW signal along the fall–winter–spring sea ice edge forming around Antarctica each year. We began by displaying time–longitude diagrams of interannual SST, SIE, ECD, ECI, and SLP anomalies along the sea ice edge. All five variables displayed the familiar characteristics of the ACW eastward from 30° to 110°E (White and Peterson 1996), with low SLP anomalies collocated with increased extratropical cyclone density and intensity in the fall–winter–spring synoptic storm aggregate. Next, we displayed corresponding time–longitude diagrams of interannual SIE, Q_E , PCP, D_{850} , and D_{200} anomalies along the sea ice edge. Again, these five variables displayed the standard ACW characteristics from 30° to 110°E , with retracted SIE anomalies collocated with greater upward latent heat flux and higher precipitation, low-level divergence, and upper-level divergence, the latter associated with deep convection. Thus, anomalous circulation throughout the troposphere propagated eastward with this ACW signal along the fall–winter–spring sea ice edge.

To establish the thermodynamics governing the troposphere response to anomalous SIE-induced latent heat flux and precipitation, we diagnosed the anomalous thermal and potential vorticity budgets of this ACW signal. In the thermal budget, we found anomalous SIE-induced latent heat flux and precipitation driving mid-to-upper-level diabatic heating and low-level cooling, similar to that observed along the northern track of the ACW (White and Chen 2002). We found the upper-layer diabatic heating balanced by vertical thermal advection and low-level diabatic cooling balanced by net horizontal thermal advection, together yielding ascending motion throughout the column and poleward wind at the low level. In the potential vorticity budget, we found the vertical gradient of diabatic heating balanced mainly by net horizontal vortex tube advection at the lower level and absolute vorticity advection at the upper level. This revealed a hybrid response of the troposphere circulation to anomalous SIE-induced diabatic heating; that is, with an equivalent barotropic meridional wind response deriving from a thermal balance at the low level and a vorticity balance at the upper level, summarized in a schematic diagram (Fig. 8).

The principal difference between this *deep diabatic heating* scenario in the ACW along the sea ice edge near 63°S and that along the Subtropical Front between 30° and 45°S (White and Chen 2002) lies in the relative intensity of the anomalous meridional advection of mean temperature at the low level in the thermal budget

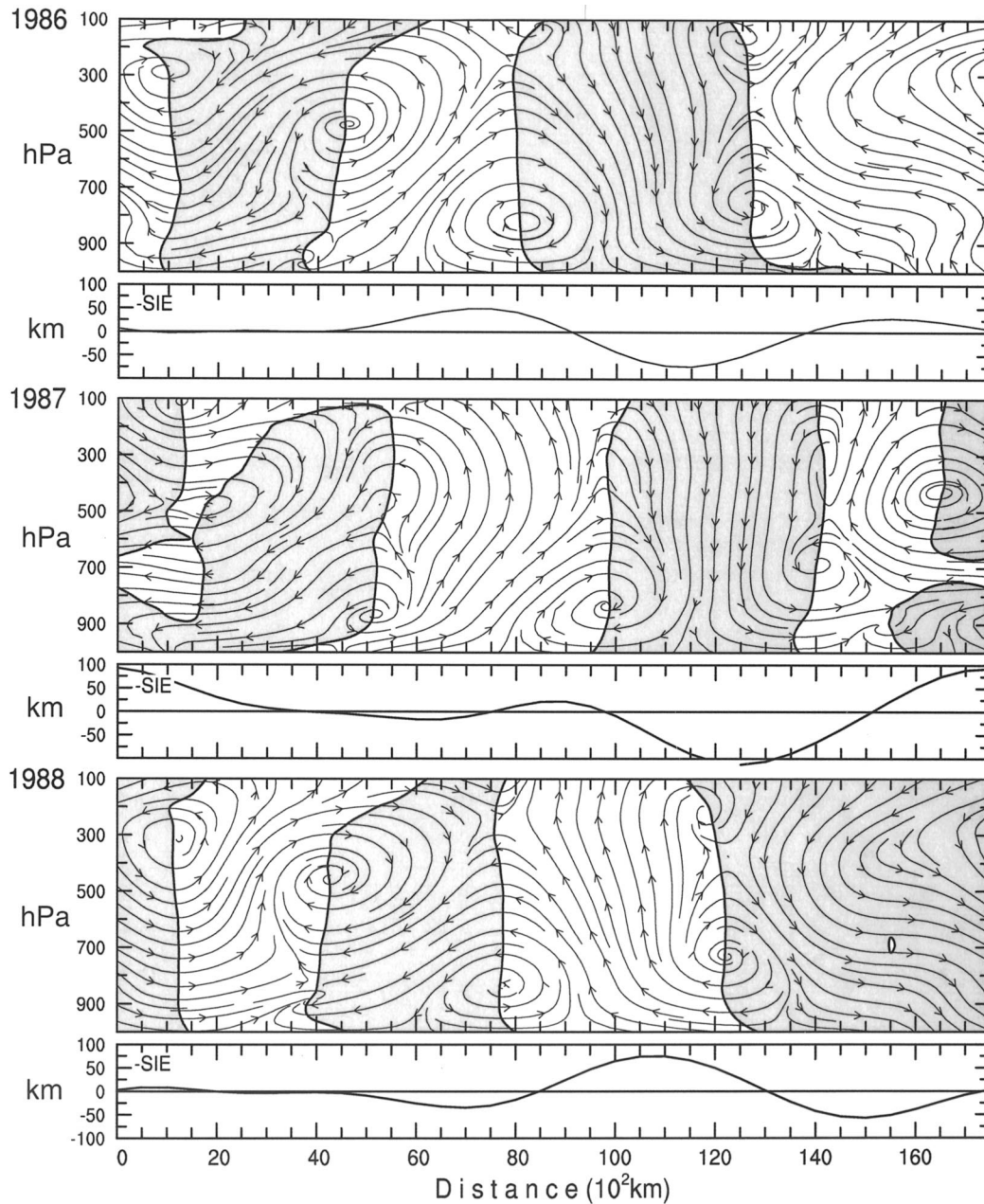


FIG. 6. Zonal-vertical sections of anomalous divergent wind in the ACW along the mean fall-winter-spring sea ice edge (using the 50% SIC criterion) for Jul 1986, 1987, and 1988. Zonal sections are measured in distance along the sea ice edge over 17 500 km, extending upward from 1000 to 100 hPa and extending eastward around the globe from 30° to 30°E (Fig. 3a). Shaded (unshaded) regions indicate anomalous descent (ascent). Streamlines connect the distribution of anomalous divergent wind velocities using the NCAR graphics package (Middleton-Link et al. 1995). Below each section is the zonal profile of interannual $-SIE$ anomalies. Retracted (expanded) SIE anomalies are positive (negative). The three maps show the eastward propagation of the anomalous zonal cells in the ACW along the sea ice edge over 3 yr, with anomalous ascent/descent collocated with retracted/expanded SIE anomalies. Vertical and horizontal divergent wind anomalies are scaled by depth of the column and horizontal radius of the cell, respectively. Vertical (zonal) wind speeds range over $\pm 0.0013 \text{ m s}^{-1}$ ($\pm 0.40 \text{ m s}^{-1}$).

and the corresponding anomalous meridional advection of mean vortex tubes in the potential vorticity budget. In both budgets along the sea ice edge, these advective components are 2–3 times larger than over the Sub-

tropical Front. Thus, along the sea ice edge the net horizontal advection of vortex tubes at the low level dominates the net advection of absolute vorticity in the potential vorticity budget, while along the Subtropical

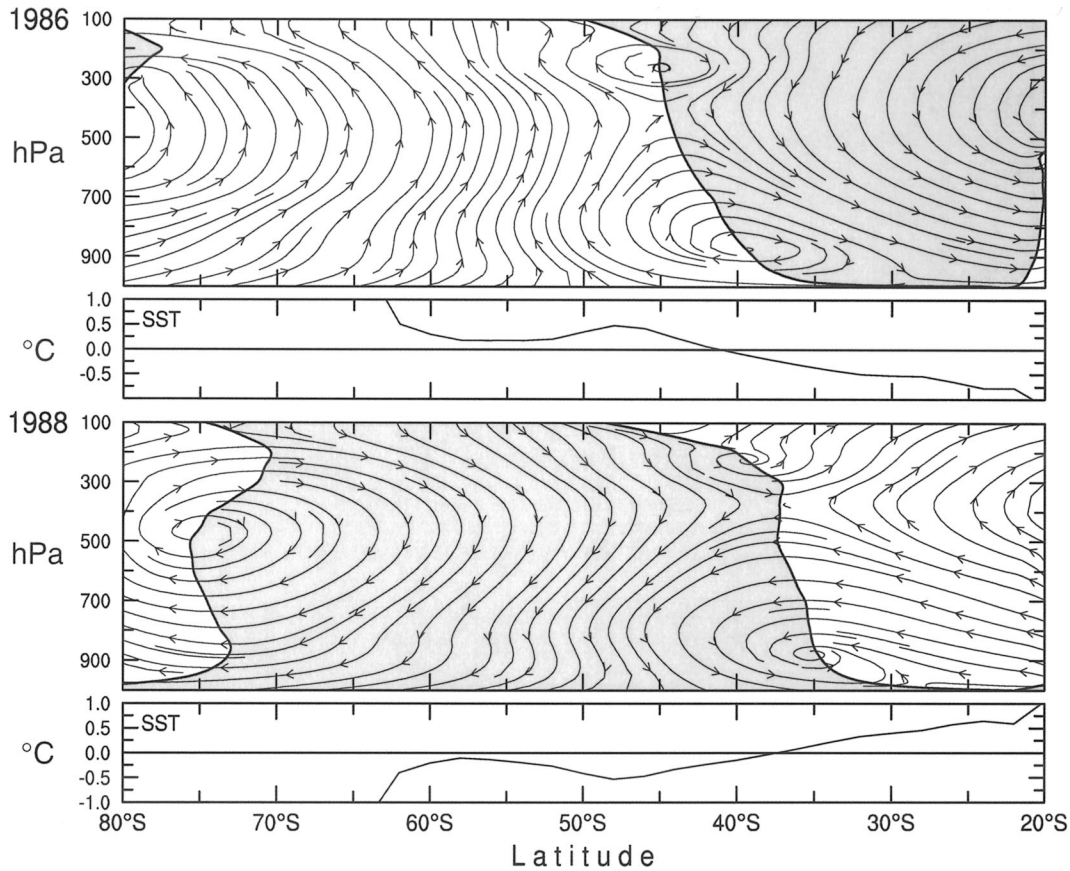


FIG. 7. Meridional-vertical sections of anomalous divergent wind in the ACW, extending upward from 1000 to 100 hPa and extending meridionally from 80° to 20°S along 180° longitude for Jul 1986 and 1988. The shaded (unshaded) regions indicate anomalous descent (ascent). Streamlines connect the distribution of anomalous divergent wind velocities using the NCAR graphics package (Middleton-Link et al. 1995). Below each section is the meridional profile of interannual SST anomalies. The two maps show the two different phases of anomalous meridional (Ferrell) cells responding to covarying SST and SIE anomalies in the ACW at the sea ice edge in the Ross Sea (Fig. 2). Vertical and horizontal divergent wind anomalies are scaled by the depth of the column and the horizontal radius of the cell, respectively. Vertical (meridional) wind speeds range over $\pm 0.0013 \text{ m s}^{-1}$ ($\pm 0.55 \text{ m s}^{-1}$).

Front both advection terms are comparable (White and Chen 2002). This difference occurs because of the stronger background temperature gradient in the lower troposphere across the fall–winter–spring sea ice edge than across the Subtropical Front.

An outstanding question concerns the source of anomalous SIE-induced mid-to-upper-level heating and low-level cooling. This diabatic heating profile derives from some combination of release of latent heat through anomalous condensation and the net radiational heating from anomalous cloud fraction (Roads et al. 1998). One likely scenario goes like this; that is, low-level radiational cooling attends upper-level latent heat release when an abnormal number of high towers are generated in individual extratropical cyclones within the synoptic storm aggregate (White and Chen 2002). This scenario now seems more likely since we found low SLP anomalies in the ACW along the sea ice edge associated with increased extratropical cyclone density and intensity in the fall–winter–spring synoptic storm aggregate. This

indicates that low SLP anomalies in the ACW are a proxy for increased extratropical cyclone activity. Further support for this hypothesis is given by the zonal phase relationship between greater PCP and low SLP anomalies, the former displaced $\sim 90^\circ$ of phase to the east of the latter, similar to that occurring in individual extratropical cyclones (Browning 1990). Thus, it appears that extratropical cyclone activity near the sea ice edge is significantly affected by changes in SIE with amplitudes $O(100 \text{ km})$ and wavelength scales $O(4500 \text{ km})$. This remains to be tested in an ocean–atmosphere–cryosphere coupled model capable of significant synoptic storm development.

A feedback from atmosphere to ocean was observed in the diagnostics of the thermal budget of the ACW along the sea ice edge. Maximum low-level diabatic cooling was observed displaced $\sim 45^\circ$ of phase to the east of retracted SIE anomalies, balanced principally by a warming tendency from the anomalous meridional advection of mean temperature. Farther to the east, this

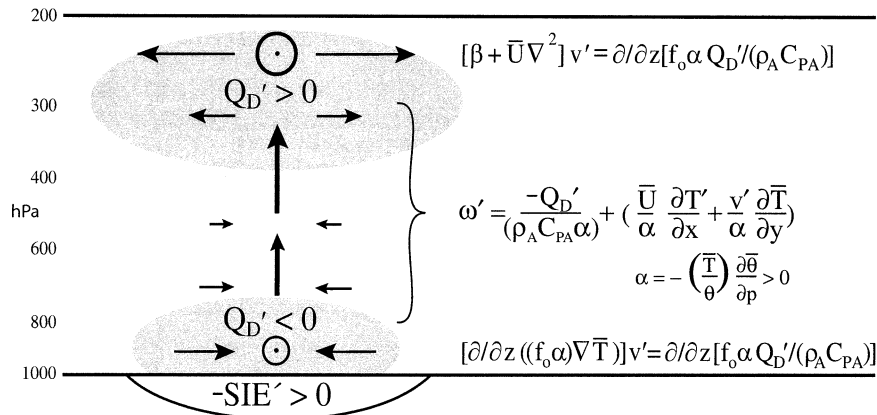


FIG. 8. A schematic diagram constructed along a zonal-vertical section of the troposphere that summarizes the *deep diabatic heating* scenario operating in the ACW along the sea ice edge. Anomalous SIE-induced latent heat flux and precipitation anomalies are associated with anomalous mid-to-upper level diabatic heating ($Q_D' > 0$) and anomalous low-level diabatic cooling ($Q_D' < 0$). This profile of diabatic heating is balanced by a combination of vertical and horizontal temperature advection, yielding anomalous ascent and poleward wind over the column. The ascending motion ($-\omega'$) achieves maximum value near 500 hPa and is associated with weak low-level convergence and strong upper-level divergence. The weak low-level convergence is balanced principally by the meridional advection of planetary vorticity in the vorticity budget, yielding poleward low-level wind. But these winds are weak compared to those associated with the anomalous meridional advection of mean temperature in the thermal budget. This conclusion is confirmed when both effects are combined in the potential vorticity budget. On the other hand, the anomalous upper-level divergence is balanced principally by the mean advection of anomalous relative vorticity, yielding poleward upper-level wind anomalies. Together, these thermal and vorticity balances at the low and upper level, respectively, yield an equivalently barotropic meridional wind response to anomalous SIE-induced deep diabatic heating in the potential vorticity budget.

low-level diabatic cooling is associated with anomalous downward latent heat flux, the latter driving an anomalous warming tendency in the upper ocean. Since the latter is displaced $\sim 90^\circ$ of phase to the east of retracted SIE anomalies, it contributes to the eastward phase propagation of this ACW signal along the sea ice edge. This phase displacement is greater than that observed in the broadscale ACW along the Subtropical Front where low-level diabatic cooling is associated with anomalous downward latent heat flux $\sim 45^\circ$ of phase to the east of warm SST anomalies (White and Chen 2002).

We found anomalous SIE-induced deep convection in the troposphere along the fall-winter-spring sea ice edge driving anomalous meridional Ferrell cells equatorward from the sea ice edge and anomalous zonal cells zonally along the sea ice edge. In zonal vertical sections of anomalous divergent wind, neighboring retracted and expanded SIE anomalies in the ACW signal along the sea ice edge were teleconnected via corresponding zonal tropospheric cells. These are similar to zonal Walker cells teleconnecting warm and cool SST anomalies associated with ENSO in the tropical Indo-Pacific Ocean (Bjerknes 1969). In meridional vertical sections of anomalous divergent wind anomalies in the ACW signal, extending from the Ross Sea to the North Island of New Zealand, warm SST anomalies (and retracted SIE anomalies) at the sea ice edge were found to be teleconnected to cool SST anomalies in the ACW along the

Subtropical Front near 30°S . Thus, the ACW signal along the sea ice edge in the Ross and Amundsen Seas were teleconnected to the ACW signal along the Subtropical Front in the western and central Pacific sectors of the Southern Ocean via anomalous Ferrell cells. It remains to determine the three-dimensional character of these Ferrell/Walker cells: that is, how they tie into the global spiral pattern of the covarying SST and SLP anomalies in the ACW over the Southern Ocean (White et al. 1998).

Acknowledgments. Warren White was supported by the National Science Foundation (Grant OCE-9920730). He was also supported by the NOAA/Office of Global Programs (Grant NOAA NA 17RJ1231) through the Experimental Climate Prediction Center at SIO, and by the National Aeronautics and Space Administration (NASA) under Contract JPL 1205106. Per Gloersen was supported by NASA, Headquarters Office of Earth Science Research Division. Ian Simmonds was supported by the Australian Antarctic Science Grant and by the University of Melbourne. Discussions with D. Cayan and S. Chen were most helpful and deeply appreciated. Our thanks extend to Ted Walker who provided the computational support and to Andrea Fincham who developed the final figures.